# A simultaneous CH4 and CO2 flux quantification method for industrial site emissions from in-situ concentration measurements on-board an Unmanned Aircraft Vehicle

Jean-Louis Bonne[1], Ludovic Donnat[2], Grégory Albora[1], Jérémie Burgalat[1], Nicolas Chauvin[1], Delphine Combaz[1], Julien Cousin[1], Thomas Decarpenterie[1], Olivier Duclaux[2], Nicolas Dumelié[1], Nicolas Galas[2], Catherine Juery[2], Florian Parent[1], Florent Pineau[2], Abel Maunoury[2], Olivier Ventre[2], Marie-France Bénassy[2], Lilian Joly[1]

[1]GSMA UMR 7331, Univerisité de Reims Champagne-Ardenne, CNRS, Reims, 51100, France
[2]Air Quality Laboratory, TotalEnergies R&D, Solaize, 69360, France

*Correspondence to*: Lilian Joly (lilian.joly@univ-reims.fr), Jean-Louis Bonne (jean-louis.bonne@univ-reims.fr)

## Abstract

We developed an innovative tool to quantify $CO_2$ and $CH_4$ emissions at the scale of an industrial site, based on a mass balance approach relying on a newly developed light-weight (1.4 kg) open path laser absorption spectrometer operable on-board Unmanned Aircraft Vehicles (UAVs). This spectrometer simultaneously records in situ $CO_2$ and $CH_4$ concentrations at high frequency (24 Hz in this study) with precisions of 10 ppb for $CH_4$ and 1 ppm for $CO_2$ averaged at 1 Hz. The large range of measurable concentrations, up to 1000 ppm for $CO_2$ and 200 ppm for $CH_4$, makes this analyzer suitable for operation on industrial sites at a short distance from the emission sources, therefore avoiding many logistical and legal limits associated with most long-range airborne observations. To quantify the emissions, high spatial resolution atmospheric concentration measurements obtained throughout a plume cross-section downwind of a source within the limited UAV flight period are exploited by calculations using a mass balance approach. This high spatial resolution, allowed by the high acquisition frequency, limits the use of horizontal interpolation, thus gaining in precision compared to current airborne alternative quantification techniques.

A field validation campaign, conducted on the TotalEnergies TADI test platform at Lacq, France, consisted in controlled $CO_2$ and $CH_4$ leak experiments to which several institutes participated with various measurement systems (gas LiDAR, multispectral camera, infrared camera including concentrations and emissions quantification system, acoustic sensors, ground mobile and fixed Cavity RingDown Spectrometers). Our method was proved suitable to detect leaks during controlled release experiments with emission fluxes down to 0.01 g s$^{-1}$, with 24 % of estimated $CH_4$ fluxes within the -20 % to +20 % error range, 80 % of quantifications within the -50 % to +100 % error range and all of our results within the -69 % to +150 % error range. Such precision levels are better ranked than current top-down alternative techniques to quantify $CH_4$ at comparable spatial scales. Observations across the plume of two offshore oil and gas platforms operated by TotalEnergies in the North Sea were used to quantify the instantaneous greenhouse gases emissions of these facilities and are coherent with reference emissions for these platforms estimated by mass balance and combustion calculations for $CO_2$. The operational deployment of such instruments and quantification methods, on a large scale and on a regular basis, potentially with fully autonomous UAVs, will allow the quantification of the time dependent greenhouse gases emissions of numerous oil and gas facilities.

## 1   Introduction

After $CO_2$, methane is currently the second most important anthropogenic greenhouse gas in terms of climate

40   forcing (Etminan et al., 2016), with effective radiative effects between 1750 and 2019 of 0.54±0.11 W m$^{-2}$ for

$CH_4$ compared to 2.1±0.26 W m$^{-2}$ for $CO_2$ (Forster et al., 2021). Methane was brought to the centre of the political

debate, with new pledges of parties to consider further actions to reduce non-carbon dioxide greenhouse gas

emissions by 2030 (Glasgow Climate Pact | UNFCCC, 2021). Due to its short lifetime of 11.8±1.8 years in the

atmosphere (Forster et al., 2021), reducing $CH_4$ emissions would be effective in terms of climate mitigation on

45   short timescales (Shindell et al., 2012): fossil $CH_4$ emissions have a global warming potential of 82.5±25.8 over

20 years, but of 29.8±11 over 100 years, in comparison with $CO_2$ with reference global warming potential of 1.0

(Forster et al., 2021). Climate mitigation actions including fast and deep methane emissions reduction would limit

climate overshoot linked with concomitant decrease of climate cooling aerosols emissions (Masson-Delmotte et

al., 2018). Large uncertainties exist in the variations of many methane anthropogenic and natural sources and sinks

50   (Saunois et al., 2020). A recent study indicates that anthropogenic fossil $CH_4$ emissions may have been

underestimated by about 25 to 40 %, representing about 38 to 58 Tg $CH_4$ per year (Hmiel et al., 2020).

According to inventories, Oil and gas (O&G) sector would be responsible for 22 % of the global anthropogenic

methane emissions (Saunois et al., 2020). O&G facilities can emit methane from multiple sources (high elevation

stacks and flares; common or local vents; fugitive sources) of different nature (process venting; incomplete

55   combustion during flaring, power generation, heating, etc; unintentional leaks) (Oil and Gas Methane Partnership

(OGMP) 2.0 Framework, 2022). O&G operators currently report their methane emissions to their stakeholders,

based on calculations using bottom-up approaches (Ng et al., 2017), including flow meters inside the plant,

emission factors, modelling and Leak Detection And Repair (LDAR) campaigns. Such methods hardly capture

temporal variations of emissions, unexpected operations and are furthermore poorly adapted to fugitive or diffuse

60   emissions. This is an important issue as recent estimates suggested that fugitive emissions represent a significant

part of emissions from O&G activities and could be strongly underestimated (Alvarez et al., 2018). Fugitive

emissions might have been increasing in recent year, which would partly explain the global methane atmospheric

concentrations increase observed since the mid-2000s (Worden et al., 2017).

Top-down approaches, based on atmospheric measurements, can complement and validate bottom-up flux

65   estimates. Developing technics able to be implemented on industrial facilities are necessary, either for fast leak

detection or for quantification of long-term greenhouse gases emissions. They should be validated via controlled

release experiments, which can be organized within intercomparison campaigns (Ravikumar et al., 2019; Feitz et

al., 2018). Such controlled release campaigns are for example organized yearly on the TotalEnergies Anomaly

Detection Initiatives (TADI) infrastructure in Lacq, southwestern France (43.41°N, -0.64°W), an industrial area

70   dedicated to the simulation of a real-size oil and gas facility, used by international groups to validate their emission

detection or quantification techniques (Kumar et al., 2021; Druart et al., 2021).

At the facility scale, different top-down emissions quantification approaches already exist, relying on both in situ

and remote sensing measurements. Some methods, well adapted to emissions quantification on flat terrains such

as landfills, like eddy covariance, stationary mass balance methods, radial plume mapping (Mønster et al., 2019),

75   cannot be adapted to all industrial contexts with complex topography and high elevation sources. In situ

atmospheric concentration measurements can be operated from the surface, with analysers at a fix position or on

mobile platforms such as in cars for onshore facilities (Brantley et al., 2014; Ars et al., 2017; Feitz et al., 2018; Yacovitch et al., 2020; Kumar et al., 2021) or on-board ships for offshore facilities (Nara et al., 2014; Riddick et al., 2019; Yacovitch et al., 2020). Other methods based on airborne observations have the advantage of measuring

80 concentrations directly inside the plume. Observations can be performed from aircrafts for onshore (Terry et al., 2017; Hirst et al., 2013; Lee et al., 2018; Conley et al., 2016, 2017; Gorchov Negron et al., 2020) or offshore facilities at the scale of an individual platform or of a whole basin (Gorchov Negron et al., 2020; France et al., 2021; Fiehn et al., 2020), but with a high logistical and financial cost, and at a long distance from sources. Observations at a long distance from the source (such as onboard aircrafts), or on slow moving platforms (such as

85 onboard ships or cars) face difficulties linked to the changing plume direction during the measurement period (also limited by the roads infrastructure for cars). Contaminations by nearby sources are also possible in such configurations. UAV-based observations are adapted to the scale of industrial facilities, including offshore, and bring different solutions to the constraints of these different types of solutions: UAVs would operate at lower costs, at high speed and directly inside the plumes at shorter distances from the sources. UAVs being able to operate at

90 short distance from the sources, they have additional advantages compared to observations at higher distances (via aircrafts or boats): they allow an easier validation of the method with controlled release experiments, they induce a gain in sensitivity as the distance to the source can be shortened to lower the effect of dilution of effluents and they have the possibility to fly inside industrial sites which permits to better localize the emission sources.

For quantifying emission fluxes based on airborne concentration measurements, two main approaches are

95 generally adopted. The first approach is based on the inversion of modelled Gaussian plumes (Hirst et al., 2013; Lee et al., 2018; Shah et al., 2020). The Gaussian-based inversion methods are commonly applied to ground mobile observations (Brantley et al., 2014; Kumar et al., 2021) or to localize multiple unknown sources (Hirst et al., 2013; Huang et al., 2015; Brereton et al., 2018). Recent UAV-based experiments relied on a near-Gaussian inversion approach but so far suffer from important uncertainties (Shah et al., 2020), which might be improved in future

100 (adapted measurement protocol or quantification model). The second approach is a mass balance method consisting in comparing the fluxes of gas entering and exiting a box around a source. It does not rely on any atmospheric model but is a direct quantification of the flux based on its integration through a surface. The main difficulties associated with this method are of being able to measure the concentrations throughout the whole plume and of having a precise knowledge of the wind conditions. This type of approach was originally employed

105 for LiDAR Dial quantifications, providing state-of-the-art Volatile Organic Compounds (VOC) quantification in complex industrial plant (NF EN 17628, 2022), and was already applied to greenhouse gases emissions quantification at various scales from industrial sites to large cities based on UAV or aircraft observations (Mays et al., 2009; Karion et al., 2015; Nathan et al., 2015; Allen et al., 2019; Fiehn et al., 2020; Morales et al., 2022). Contrary to Gaussian-based inversion models, mass balance does not require the assumptions of constant and

110 continuous emissions creating a steady-state system with normally distributed pollutant concentrations over a flat and uniform terrain, which is often none applicable to onshore or offshore fields.

Identification and quantification of $CO_2$ and/or $CH_4$ sources via top-down UAV-based approaches require instruments with high-quality measurements of $CO_2$ and $CH_4$ in a large range of concentrations and with a very

115 low response time to operate at high frequency. Different types of methane sensors suitable for UAV-sampling already exist. Metal oxide gas sensors (Neumann et al., 2013; Malaver et al., 2015; Liu et al., 2020; Rivera

Martinez et al., 2021) or cryptophane-A cladded Mach-Zehnder interferometers (Dullo et al., 2015) are compact and competitive in price but with a relatively high detection limit and low response time (17 ppm of $CH_4$, 10 s response time) (Dullo et al., 2015). Miniaturised laser-based sensors also emerged in the last years (Berman et al.,

120    2012; Khan et al., 2012; Golston et al., 2017, 2018; Nathan et al., 2015; Shah et al., 2020; Rivera Martinez et al., 2021; Tuzson et al., 2020), but do not necessarily have a large sensitivity range, a low response time and a light weight below 2 kg and generally measure only one species. Tunable Diode Laser Absorption Spectroscopy (TDLAS) allows a high selectivity and sensitivity in the gases detection and is considered as the most advantageous technique for measuring atmospheric gas concentrations (Durry and Megie, 1999). Many applications are already

125    based on this technique, not only UAV applications, among which Cavity Ring-Down Spectroscopy (CRDS) (Crosson, 2008; Chen et al., 2010; Rella, 2010), Cavity Enhanced Absorption Spectroscopy (CEAS) (Romanini et al., 2006), Integrated Cavity Output Spectroscopy (ICOS) (O'Keefe, 1998; O'Keefe et al., 1999) or the most straightforward Direct Absorption Spectroscopy (DAS) (Xia et al., 2017). Open cavity instruments have the advantage of increasing the response time compared to closed cavity instruments. DAS is well adapted to in situ

130    measurements and can be applied to sensors light enough to be embarked on UAVs, which led to the choice of technology adopted for the development of the sensor presented in this study.

In this study, we present a newly developed UAV-embarked $CO_2$, $CH_4$ and $H_2O$ in situ analyser and a methodology of emissions quantification adapted to the monitoring of O&G facilities. We present the characterization of this analyser for the environmental conditions of its field applications. Our emissions quantification method has been

135    validated against $CH_4$ controlled releases in an intercomparison effort during the TADI campaigns of 2019 and 2021, together with other quantification methods using varied technologies: multispectral camera, ground based CRDS (fix stations or mobile measurement in a car), wind and gas LiDAR, infrared camera including concentrations and emissions quantification system, or Tunable Diode LiDAR. As a large part of TotalEnergies production activities are offshore-based, we present an application of our method to the quantification of emissions

140    of two offshore gas production platforms in the North Sea.

## 2    $CO_2$, $CH_4$ and $H_2O$ analysers for UAV in situ observations

### 2.1    Technical description

A new sensor has been developed for in situ $CO_2$, $CH_4$ and $H_2O$ observations able to operate on-board UAVs (see Figure 1): the Airborne Ultra-light Spectrometer for Environmental Application (AUSEA). It is based on the

145    technical concept of the AMULSE instrument (Joly et al., 2016, 2020). As for the AMULSE instrument, the AUSEA instrument includes an open-path infrared Laser absorption spectrometer using two DFB interband cascade laser diodes in the mid-infrared spectral region (NIR): near 4 µm with a direct path of 11 cm to measure $CO_2$ concentrations and near 3 µm in a home-made Herriott multipass cell of 3.5 m path length to measure $CH_4$ concentrations. The measurement frequency is of 24 Hz.

150    Compared to the AMULSE instrument, the AUSEA instrument has been adapted to reduce its weight, to adapt its sensitivity range to industrial applications (up to 1000 ppm in $CO_2$ and up to 200 ppm in $CH_4$), to limit the effect of vibrations, air turbulences, magnetic perturbations and to implement air-ground communication for a real time visualisation of the concentrations by the operators. It has a power consumption of 8 to 15 W in most usual cases, depending on the external temperature (with maximal power consumption of 30 W during less than 1 s at start-

155    up). It can be powered either with dedicated batteries for an average lifetime of 1.5 hours or directly by the UAV. The instrument also embarks an IMET 4 from InterMet Systems (modified to fit in the instrument) to record air temperature, pressure and relative humidity at 1Hz frequency, a LiDAR Lightware LW20/C to measure the distance to the ground and a GPS for position and time recording. Altogether, the weight of the AUSEA sensor has been optimized down to 1.4 kg, including all previously listed hardware.

160    Two AUSEA instruments (hereafter named AUSEA111 and AUSEA112) have been used for laboratory tests and field applications presented in this study, in order to verify the reproducibility of performances between several analysers.

### 2.2    In-lab $CO_2$ and $CH_4$ analysers characterisation

In-lab characterisation of the stability and linearity was performed independently on AUSEA111 and AUSEA112
165    instruments, and repeated at different periods in 2021 and 2022. For these experiments, each AUSEA instrument was placed in a custom-made atmospheric chamber in which air is continuously mixed and homogenised (using fans) and temperature is regulated (at laboratory temperature).

#### 2.2.1    Stability

The stability experiments consisted in measuring the same air sample within the closed atmospheric chamber by
170    the AUSEA instrument over several hours. For AUSEA112, two experiments are exploited (conducted on 2022-04-19 for a duration of 3 hours and 2 minutes and of 1 hour and 13 minutes); while four experiments are exploited for AUSEA111 (two were conducted on 2022-06-08 for respective durations of 1 hour and 35 minutes and of 15 hours and 12 minutes and two were conducted on 2022-03-23 for respective durations of 50 minutes and 1 hour and 50 minutes).

175    Allan deviation, calculated from those experiments for both analysers, are presented in Figure 2 and Table 1. The precision of our measurements can be derived from these experiments: for $CH_4$, precisions are below 20 ppb at 2 Hz, below 10 ppb at 1 Hz, below 1 ppb at 10 s and below 0.2 ppb at 1 minute; for $CO_2$, precisions are below 2 ppm at 2 Hz, below 1 ppm at 1 Hz, below 0.1 ppm at 10 s and of 0.01 ppm at 1 minute. We note a minimum of precision for the instrument AUSEA112 at 60 seconds with a stagnation of performances for longer averaging
180    periods, contrary to the instrument AUSEA111 which has a better longer-term stability.

#### 2.2.2    Linearity

To evaluate linearity, air samples of varying concentrations were simultaneously measured by the AUSEA analyser placed in the atmospheric chamber and by a reference instrument pumping air from the atmospheric chamber. An air with high $CH_4$ concentration was initially injected in the atmospheric chamber and progressively
185    mixed with room air, thus spanning a continuous range of concentrations from the initial sample up to ambient air levels. Variations of $CO_2$ concentrations were simply generated by natural variations of the $CO_2$ values in the laboratory air. The reference instrument used was a Cavity Ring-Down Spectrometer (Picarro Inc. model G2401), hereafter referred as Picarro, with an operating range certified by the manufacturer from 0 to 1000 ppm for $CO_2$ and from 0 to 20 ppm for $CH_4$. The Picarro has been validated through the ICOS Atmospheric Thematic Center
190    protocol (Yver Kwok et al., 2015) and was calibrated using the standard procedure for ICOS atmospheric monitoring stations with 4 calibration standards of known $CO_2$ and $CH_4$ concentration ranging from 396.05 to

504.16 ppm for $CO_2$ and 1807.7 to 2346.5 ppb for $CH_4$ (ICOS RI, 2020). AUSEA and Picarro analysers data were compared at the Picarro temporal resolution of 5 seconds. Linearity experiments were conducted on 2022-03-23 and 2022-06-08 for AUSEA111 and on 2021-04-15 and 2022-04-19 for AUSEA 112. Linearity experiment

195    covered $CO_2$ and $CH_4$ concentrations ranging from 429.0 to 861.4 ppm of $CO_2$ and from 2.1 to 20.00 ppm of $CH_4$ (within the reference instrument certified linearity domain).

The results of the linearity experiments are presented on Figure 3 and Table 2. An excellent linearity was observed for both species for each experiment: linear regressions provide excellent coefficients of determination $R^2$ of 1.0 for $CH_4$ and $CO_2$, with p-values (probability of obtaining tests results at least as extreme as the results actually

200    observed) well below $10^{-5}$, so with high statistical validity. Low residuals are observed for each linear regression (difference between measured values and linear regressions): within 0.02 ppm of $CH_4$ and 1.5 ppm of $CO_2$ (Figure 3), which corresponds to the precisions of the instruments and do not reveal deviations from a linear distribution. We observed relatively low variations of the slopes and intercepts of the linear regressions between repeated experiments over the course of several months (Table 2), therefore of the instrument response (slopes and

205    intercepts variations respectively below 2.3% and 0.16 ppm for $CH_4$ and 1.6% and 7 ppm for $CO_2$).

The linearity of our AUSEA sensor was experimentally validated for $CO_2$ concentrations between 429.0 and 861.4 ppm and $CH_4$ concentrations between 2.1 and 20 ppm, against the guaranteed linearity domain of a reference instrument validated top-of-the-art metrology standards (Yver Kwok et al., 2015) . However, the sensitivity domain of our AUSEA sensor exceeds these limits: the chosen pathlength for the $CH_4$ measurements, has been

210    determined to reach saturation around 200 ppm. Given the saturation of the $CO_2$ absorption spectrum, the maximum of measurable concentration is limited to 1000 ppm (but this limit can be easily adapted by modifying the $CO_2$ laser-to-detector pathlength). Therefore, we believe the linearity domains also exceed the range of concentrations tested in the laboratory, up to 1000 ppm for $CO_2$ and above 100 ppm for $CH_4$. The lack of a reference instrument with a comparable certified linearity domain in our laboratory did not allow us to validate

215    this limit so far. However, additional linearity experiments conducted with the same reference CRDS instrument, not presented here, for $CH_4$ concentrations up to 100 ppm also depicted an excellent linearity (also with $R^2$ of 1.0 and $p<10^{-5}$ for 24975 data points), therefore giving confidence in the linearity of our AUSEA sensors, even for concentrations out of the CRDS instrument manufacturer's certified linearity domain. This confidence is also motivated by the fact that the same type of CRDS analysers were also employed for the quantification of industrial

220    emissions of $CH_4$ with peaks up to approximately 90 ppm (Kumar et al., 2021; Jackson et al., 2014).

### 3   Source emissions quantification

A mass balance method has been developed to quantify source emissions from atmospheric concentration measurements. It relies on the airborne monitoring of atmospheric concentrations of the species of interest from UAV and of the wind speed and direction at the elevations of the UAV.

225

### 3.1 Monitoring method

#### 3.1.1 Measurements on-board Unmanned Aircraft Vehicles

The AUSEA instrument is embarked on a low-weight (below 8 kg payload) commercial multicopter. Several models of UAVs have been employed (DJI M200, DJI M210, DJI M300, and a non-commercial drone), able to flight under wind speeds up to 12 m s⁻¹, with autonomies of 20 to 45 minutes. The instrument was always integrated between both UAV landing gears, below the propellers level (see Figure 1). Concentration measurements are remotely monitored in real-time by the operators on the ground (usually a pilot and a co-pilot), allowing to locate the plume and optimize the trajectory of the UAV to fit to the flight plan requirements of the emissions quantification method.

#### 3.1.2 Wind profiles meteorological parameters measurements

Wind speed and direction profiles are recorded by a commercial ZX300 Doppler wind LiDAR (from ZX LiDARs Inc.), equipped with an AIRMAR weather station at 2.5 m above ground level (or m.a.g.l.). The LiDAR records wind speed and direction at 10 elevations between 11 and 300 m.a.g.l., completed by wind measurements at the AIRMAR station, thus covering the range of altitudes of the UAV tracks. The AIRMAR station also records temperature, relative humidity and air pressure. Wind speed measurements have an approximate 15 to 20 s time resolution and a precision of 0.1 m s⁻¹ and 0.5°. The wind speed and direction are interpolated at the elevations of the UAV. For elevations below the first height of LiDAR measurements, a logarithmic interpolation with assumption of null wind speed at the ground level is used, following the shape of a neutral wind profile. For levels above the first LiDAR measurement height, the interpolation is linear.

#### 3.1.3 UAV flight protocol

Our protocol for UAV-based atmospheric concentrations monitoring was designed for our quantification model. The UAV flight plan should meet the conditions described hereafter (see Figure 4). Concentration measurements are performed under the wind of the sources, within a vertical plane crossing the plume, later referred as the observational plane. The observational plane must be as close as possible to a plume cross-section, therefore orthogonal to the prevailing wind direction. Several horizontal transects covering the entire plume and part of the surrounding background are recorded within this plane, with elevations distributed from below (or closest to the ground possible) to above the plumes. A precise wind speed and direction monitoring covering the range of altitudes of the UAV must be conducted simultaneously.

### 3.2 Emissions quantification model

In the mass balance approach, the emission rate $Q$ (in g s⁻¹) is estimated from a flux through the observational plane crossing the plume of emissions. It assumes constant emissions during the monitoring period and no degradation of effluents through chemical reactions over the monitoring period, which is reasonable for $CO_2$ and $CH_4$. The referential $x, y, z$ is defined by the observational plane (see Figure 4), with $x$ in the horizontal direction orthogonal to the plane, $y$ in the horizontal direction along the plane and $z$ in the vertical direction. $Q$ is equal to

the integral across the plane, of the wind speed component along $x$, $u_x(y,z)$ (in m s$^{-1}$) multiplied by the differential of volume concentrations between the plume $c_p(y,z)$ and the background $c_{bg}(y,z)$:

$$Q = \iint_{y,z} u_x(y,z) \cdot [c_p(y,z) - c_{bg}(y,z)] \, dydz \, , \qquad (1)$$

Background concentrations are assumed spatially uniform, $c_{bg}(x,y,z) = c_{bg}$ and estimated from the concentrations measured outside the plume. Wind speed is assumed horizontally uniform: $u_x(y,z) = u_x(z)$. As the wind direction might fluctuate over the complete monitoring period, we consider the average wind over the duration of each transect. Noting $\alpha(z)$ the angle, often non-neglectable in practice, between the wind direction and the orthogonal to the transect, the component $u_x(z)$ of the wind speed can be expressed as a function of the total wind speed $U(z)$, as follows: $u_x(z) = \cos(\alpha(z)) \cdot U(z)$. Altogether, Eq. (1) becomes:

$$Q = \int_z U(z) \cdot \cos(\alpha(z)) \cdot \left[ \int_y (c_p(y,z) - c_{bg}) \, dy \right] dz, \qquad (2)$$

We note $q(z) = U(z) \cdot \cos(\alpha(z)) \cdot \left[ \int_y (c_p(y,z) - c_{bg}) \, dy \right]$ the flux component at each horizontal transect level. The integral of $q(z)$ along $z$, is calculated from interpolated values of $q(z)$, assuming neglectable vertical variations of the plume compared to the vertical gap between successive transects.

This method can be applied in a wide range of meteorological conditions (limited by UAV maximum wind speeds limits), but is poorly adapted to low wind speeds and unstable wind directions, where measurement uncertainty can strongly rise.

### 3.3 Validation of emissions quantification method

#### 3.3.1 Field validation protocol

Two validation campaigns were conducted from 1 to 10 October 2019 and from 07 to 10 September 2021 on the TotalEnergies Anomaly Detection Initiatives (TADI) platform in Lacq, in southwestern France (43.41°N, -0.64°W). The TADI platform, already described in the literature (Kumar et al., 2021, 2022), is an approximately 2000 m² almost flat rectangular area (Figure 5), surrounded by agricultural land and rural settlements, and important chemical and industrial plants on the east of the platform. Multiple obstacles for dispersion are created by tents where other instruments are located, decommissioned oil and gas equipment and other small infrastructures. A road surrounding the north and east borders of the site cannot be flown over, limiting the area of UAV operations.

Several emission sources were spread over the platform, within a 40x60 m rectangular area classified as "ATEX zone" (Figure 5), out of reach for all participants due to security reasons. Sources were elevated between 0.1 and 6.5 m.a.g.l, originating from a variety of equipment (valve, connector, flange, drilled plug, tank, manhole, corrosion, flare pipe - no combustion, etc.). Either $CO_2$ or $CH_4$ or a combination of both species were emitted, but also a mixture including a proportion of $C_2H_6$ or $C_3H_8$, to test if the method is able to differentiate these species from $CH_4$. Only $CH_4$ emissions quantifications results are presented in this study (the low number of $CO_2$ releases does not allow statistical analysis of our $CO_2$ quantifications). Release scenarios had durations from 10 to 73 minutes (with two short-lasting leaks of a 15 seconds and 2.5 minutes which were not be monitored with our method), with pauses of approximately 5 minutes between two releases. Mass flow controllers were used to regulate and monitor the controlled $CH_4$ flow rates, with a large range of values from 0.01 to 150 g s$^{-1}$. This variety of emission sources, duration and amplitude is representative of the diversity of emission scenarios expected on

industrial facilities. Information about the leaks (locations, species and fluxes) of each experiment can either be communicated (open trials) or withheld (blind tests) from the measurement teams. Results from both open trials and blind tests are presented.

For our UAV-based emission quantification method, one team was operating a DJI M200 in 2019, while two teams were operating either a DJI M300 or a DJI M210 and a non-commercial UAV in 2021. In 2021, all drones were equipped with RTK GPS positioning systems, which was not the case in 2019. Flight durations have been from 10 to 20 minutes. Concentration measurements were performed within a vertical plane distant from the sources from approximately 20 to 80 m. As the sources were at low elevation (below 6.5 m), the plumes were monitored with a varying number of 5 to 15 low elevation horizontal transects distributed between 1 and 12 m.a.g.l. in 2019 and up to 35 m.a.g.l in 2021. Wind speeds and directions were measured at 10 elevations between 11 and 300 m.a.g.l. with the ZX300 wind LIDAR (equipped with the AIRMAR station at 2.5 m.a.g.l.).

### 3.3.2 Results of validation experiments

$CH_4$ emissions quantifications of the two TADI campaigns are analysed hereafter and compared to the reference real fluxes derived from mass flow meters at the source. The emissions quantifications for each controlled release experiment are given in the Supplementary Materials on Table S1. Statistical analyses of the results are presented in Figure 6 and Table 3.

During the two TADI campaigns, UAV measurements were conducted during 34 out of 41 controlled releases (among which 15 were blind tests) in 2019 and during 20 out of 24 controlled releases (all blind tests) in 2021. Emission quantifications could be successfully calculated with our method for respectively 26 and 18 controlled release experiments in 2019 and 2021. Some release experiments could not be quantified due to unavailability of the instruments, UAVs or pilots and some of the quantification flights were discarded as the flight paths did not match our standards (e.g. did not cover the complete horizontal or vertical plume section or technical issues were noticed with some of the sensors).

Some of the controlled releases could be monitored by several independent flights (3 by 4 flights, 4 by 3 flights, 19 by 2 flights) and the rest (19 releases) could only be monitored once. The averaged, minima and maxima of all quantifications are presented for each release experiment, as well as the relative errors of the average of quantifications compared to the reference values. Among all 45 quantifications of the TADI campaigns, the average relative error is of 7 %, the median is of -5 %, with a standard deviation of 53% (Table 3). No significant difference can be observed between quantifications of controlled release experiments based on 1, 2, 3 or 4 flights. The dispersion of results seems lower for the quantifications based on 4 flights (minimum and maximum relative errors between 19 % and 26 %), but since there are only 3 controlled release experiments based on the 4 quantifications flights, this result cannot be considered statistically valid. However, one would logically expect an improvement of precision with a higher number of quantification flights for the same source.

Figure 6 presents the averaged quantifications of all controlled release experiments compared to the real fluxes. No specific trend can be observed on the error distribution, which would depict either a decrease of precision or biases for extreme low or high fluxes.

Table 4 presents a classification of the quantifications in terms of performance classes, for different ranges of real $CH_4$ emission fluxes. The relative errors of our quantification compared to the true values show that out of 45 quantified controlled releases, 24 % relative errors between -20 and +20 % compared to the true values (11 out of

45 controlled releases, cf. Figure 6), and 80 % of our quantifications had relative errors between -50 % and +100 % (36 out 45 controlled releases, cf. Figure 6). The lowest and highest relative errors are respectively of -69 % and +149 %. There is no significant change in performance of our quantifications which would depend on the quantity of $CH_4$ emitted.

Experiments conducted during the TADI campaigns allowed to validate our emissions quantification method, which depicted similar performances for $CH_4$ emissions on a wide spectrum of fluxes, ranging from order of magnitudes between $10^{-2}$ and $10^{+2}$ $g.s^{-1}$. Absolute lower and upper detection limits are difficult to determine as they might be influenced by the conditions on the field (potential flight restrictions affecting the horizontal or vertical area covered by measurements, particular wind conditions, etc.). The possibility to modulate the flight plane distance to the source allows to adapt monitoring conditions to the signal-to-noise ratio and to the potential saturations of the concentration monitoring.

If the validation of our method has been done specifically for $CH_4$ emissions quantification, it can easily be extrapolated to the quantification of $CO_2$ emissions, as the monitoring of both species concentrations is performed with the same instrument with a sensitivity range adapted to the field applications providing similar signal to noise ratios.

During the TADI campaign, as the emission sources were situated close to the ground and as the measurements were performed at a relatively short distance, thus with low vertical mixing, most flights were performed at low elevations, in particular in 2019 (typically below 12 m.a.g.l.). In such conditions, wind profiles measurements could have been performed with alternative devices such as multiple ultra-sonics wind sensors sprayed along a vertical mast of a few meters, instead of a LiDAR measuring the first level at 11 m.a.g.l. In 2021, the distance between the flight plan and the source being generally longer than in 2019, some of the flights reached higher altitudes (up to 35 m.a.g.l.), thus requiring the use of a LiDAR. For low elevations (below the first LiDAR level) the uncertainties associated with wind speed measurements would be expected to be higher than for a within the range of levels monitored by the LiDAR, furthermore considering the logarithmic distribution of wind speed profiles. This will bring a larger uncertainty in our quantifications in the case of low plumes, such as those encountered during most of the TADI experiments. At higher elevations, we expect lower uncertainties linked with wind speed monitoring.

In addition, low wind speed conditions were often encountered, which is also challenging for emissions quantification as it is associated to more instabilities of the wind direction and thus an uneasy definition of the measurement plane. Considering these multiple suboptimal conditions, higher precisions could be expected for the monitoring of large and/or high sources such as offshore platforms, stacks or flares which rarely experience low wind conditions.

### 3.3.3    Comparison to other top-down approaches

Our performances estimated from the TADI campaigns can be compared to the performances of other top of the art technologies. As described earlier, our quantification method obtained 24 % of results between -20 and +20 % relative error compared to the true values, 80 % of results between -50 % and +100 % and all the results were within the range of -69 % to +150 % compared to the true values. Several technologies using UAVs, airplanes, or mobile ground measurements were tested and compared during the international Stanford/EDF Mobile Monitoring challenge (Ravikumar et al., 2019) at the Methane Emissions Technology Evaluation Center (METEC), in

Colorado, US and at a facility near Sacramento, California, US. The performances of our method are better than the those of the other techniques compared within this challenge: only one method (Seek Ops Inc., based on drone observations) had all quantifications between -90% and 1000%, but with only 36% of quantifications between the -50% to +100% interval; while the best performance on the -50% to +100% interval was achieved by Ball

380 Aerospace plane observations with 53% of quantifications within this range. Emitted fluxes were generally lower for the Stanford/EDF challenge (from 0 to 0.1 g s$^{-1}$ on METEC and 0 to 7 g s$^{-1}$ at Sacramento) than for our TADI intercomparison experiments (from 0.01 to 150 g s$^{-1}$), but, as stated earlier, our results are similar on a subset of experiments focusing on the lowest emitted fluxes.

Other methods for $CO_2$ and $CH_4$ sources tracking and emissions quantification include measurements with CRDS

385 analysers from cars. An evaluation of such technique coupled with an atmospheric inversion based on a Gaussian plume dispersion model has been carried out under conditions comparable with our study during a TADI intercomparison campaign in 2018 (Kumar et al., 2021). Results of this validation campaign depicted a good accuracy of the emissions quantification, with estimates of the $CH_4$ and $CO_2$ release rates with ~10 to 40 % average relative errors. But only a limited number of 16 out of 50 controlled releases could be monitored, as this technique

390 is constrained by the ability to drive through the plume, which is not possible for high elevation plumes (in cases of high stacks or plume rise) or for wind direction incompatible with the road infrastructure.

A UAV-based $CH_4$ emissions quantification method with a near-field Gaussian plume inversion model (Shah et al., 2020) obtained large uncertainties compared to our method with respective lower and upper uncertainty bounds on average of 17 % ± 10 % (1σ) and 227 % ± 98 % (1σ) of the controlled emission flux. Gaussian approaches rely

395 on hypotheses such as a well-mixed plume (problematic at a short distance from the source), a flat terrain, uniform and constant wind conditions, which are not necessarily true and may be less detrimental for mass balance approaches. The higher acquisition frequency of our analyser compared to this study is also a technical advantage which leads to better spatially resolved measurements and therefore an improved representation of the plume.

A recently published UAV-based emission quantification technique also relying on a mass bass approach (Morales

400 et al., 2022), was tested on a short range of release rates (0.26 to 0.48 g.s$^{-1}$) and obtained average bias of -1 % and RMSE of errors of +69 %. These results are comparable with the average and standard deviation of our residuals (+7 % and +53 %), which supports the validity of the mass balance method for the quantification of greenhouse gases emissions. The main differences compared to our approach was the use of only low-level sonic anemometers to measure wind speed and direction, without a real monitoring of the vertical wind profile, and the quantification

405 of $CH_4$ emissions exclusively with a heavier sensor (2.1 kg compared to 1.4 kg for our sensor).

### 3.4 Application to offshore oil and gas facilities emissions quantification

### 3.4.1 Protocol of offshore platforms monitoring campaigns

A one-day measurement campaign was conducted in the North Sea on April 2019 to quantify the emissions of two offshore platforms (hereafter named P1 and P2). These platforms are equipped with power generators and gas

410 turbines driving the compressors, both emitting $CO_2$ to the atmosphere. Stacks of gas turbine are at 50 m above sea level (m.a.s.l.) with vertical ejection, stacks of power generator are at 30 m.a.s.l with horizontal ejection. The main source of $CH_4$ emissions is the gas venting system, at 80 m above the sea surface, emitting mainly methane

with vertical ejection. Other potential minor sources of $CH_4$ are expected: fugitive emissions and unburnt $CH_4$ in the turbine smokes.

415    Measurements were carried out from a supply boat chartered on purpose by the company from Den Helder harbor, Netherlands (Figure 7,a.b.). The deck was used as a take-off and landing site for the UAV. The wind LiDAR installed on the deck recorded wind profiles at 10 levels between 15 and 300 m.a.s.l. (Figure 7,b). Real-time concentration measurements were visualized by a person assisting the pilot to adapt the UAV trajectory to the position of the plumes and manage wind direction fluctuations. The duration of each flight was of 10 to 20 minutes.

420    Each flight can be assigned to a trial in terms of concentration recording and emission calculation. The first flight is often a detection flight aiming at localizing the plume and not always usable for emission quantification. Respectively 8 and 7 repeated flights and emissions quantifications were conducted for the monitoring of both platforms (see Table S2 in the Supplementary Materials).

Our UAV-based quantifications of $CO_2$ and $CH_4$ emissions are presented as relative differences to reference values
425    for each platform, corresponding to the daily averaged emissions calculated by the platforms operator thanks to methods based on real measurements on the day of comparison, using mass balance and processing data (venting) and combustion balance (gas turbines and power generator). This emissions calculation method is expected to be reliable for $CO_2$ emissions, as it is based on reliable input data (combustion flows, gas composition, $CO_2$ conversion of hydrocarbons). For $CH_4$, this calculation method assumes the proper functioning of equipment (e.g.
430    closed valves).

### 3.4.2    Offshore platforms emissions quantifications

During this campaign, the distances between the source and the measurement plane were varying between approximately 150 and 450 m depending on the flight (Supplementary Table S2). To match the vertical distribution of the plumes, originating from sources at typical elevations around 80 m.a.s.l., horizontal transects were
435    performed within the range of 50 to 120 m.a.s.l. Figure 8 presents typical wind conditions for one flight (2_P2) of the offshore platforms emissions monitoring campaign. Stable wind directions were observed during this flight (Figure 8.a) with similar wind directions at for all horizontal transects. The absence of strong shear in the wind direction during our measurements allowed capturing emission plumes within a single measurement plane for each flight. The wind speed profile of this example is typical for this offshore campaign (Figure 8.b), with a logarithmic
440    profile below 40 m and increasing wind speeds above this limit, typical for stable atmospheric conditions.

Results of the emission quantifications of both offshore platforms are presented in Table 5. The quantified emission fluxes are presented in terms of relative difference compared to reference daily-average fluxes estimated for the platforms by mass balance and combustion calculation, thus non-representative of short-time variations of emissions.

445    For the quantification of $CH_4$ emissions, 13 flights were used mong 15 flights (7 for platform P1 and 6 for platform P2), the first flight for each platform being a short test flight to find the plume position. Mean $CH_4$ emission quantification for all 7 flights for P1 platform presents a 46 % relative difference compared to the reference vent stack expected emissions. This difference is of 12% for the P2 platform. At the time scale of individual flights, large variations in the $CH_4$ emissions quantification are observed for both platforms, with estimates varying
450    between +8 % and +128 % for the P1 platform, and between -60 and +229% for the P2 platform, compared to the daily reference emissions. For the P2 platform, the highest estimate of $CH_4$ emissions corresponds to a single flight

(+229 %) largely above the average and standard deviations value of the other 5 flights (-31 ± 18 %). The vertical profile of $CH_4$ fluxes by transect levels for this particular flight (not shown) depicts an important flux of $CH_4$ at an elevation lower than the usual main plume observed for all other flights. It is therefore reasonable to interpret this flux value as a short-time event of emissions from a different source than those used for the reference daily average estimates.

The mean values of the methane emissions quantification for all flights combined are comparable although higher than reference daily averaged emissions (+46% and +12% for P1 and P2). Our quantification method should be representative of the actual emissions of the whole platform, including fugitive emissions. Reference fluxes are based on estimation using emission factors, gas composition and flow rate measurements or estimation. The higher methane emissions of platform P1 from our method compared to the reference emissions led to a review of some of the platform processes during which an unexpected emission was detected and repaired from a defect valve. A significant emission reduction is expected after the repair. Repeated measurements would be helpful to confirm the actual improvement.

Concerning the quantification of $CO_2$ emissions, 7 flights could be exploited for platform P1, while only 4 flights are used for platform P2, as the $CO_2$ plume was not entirely captured by our flight plans during some flights, contrary to the $CH_4$ plume, as different sources are involved for both species. The $CO_2$ emissions quantifications are expressed as a relative difference to the daily averaged reference emissions. The estimated $CO_2$ emissions relative difference to the reference emissions are on average for all flights of -21 % for platform P1 and -47 % for platform P2. Emissions quantifications of each independent flight provided variable results, with minimal and maximal values of -39 to +14 % for platform P1, and between -28 % and +2 % for platform P2, thus within the precision of our quantification method. Part of the temporal variability of the $CO_2$ emissions quantification of platform P1 could also be explained by the presence of a supply vessel which arrived and left the platform during the two flights with the highest emissions quantified. Part of the quantified $CO_2$ emissions of both flights could therefore be attributed to the emissions of this supply vessel. If only the other 5 flights are considered, the averaged quantification of $CO_2$ emissions would be of -31 % ± 18 % relative difference compared to the reference value for platform P1, with a maximum value of -20 %.

Altogether, our emissions quantifications depict large variations between the different flights, for $CO_2$ and more particularly for $CH_4$ fluxes (Table 5). Such variations can be linked with real short-term variations of the emissions over the monitoring period, which are not reflected by the reference emissions values provided at a daily resolution only.

For some flights of this campaign, the measurements did not properly cover the entire plume cross-section vertically (values of $q(z)$ did not reach zero). Therefore, the plumes vertical boundaries were estimated from gaussian interpolations of the vertical distribution of $q(z)$. Better flight plans including measurements below and above the plumes would be necessary for improved quantifications and will be an important requirement of future monitoring protocols.

## 4 Conclusions

This study presents an atmospheric emissions quantification technique based on a new atmospheric $CO_2$ and $CH_4$ concentration analyser embarked under a UAV associated with a mass balance box model. The controlled release

490   campaigns on the TADI platform in 2019 and 2021 validated this method independently of the type of source or carrier, and showed better accuracy compared to other current top-of-the-art $CO_2$ and/or $CH_4$ emissions quantification techniques using either multispectral camera, ground based CRDS (fix stations or mobile measurement in a car), wind and gas LiDAR, infrared camera including concentrations and emissions quantification system, or Tunable Diode LiDAR (Ravikumar et al., 2019; Shah et al., 2020; Kumar et al., 2021;

495   Druart et al., 2021) and comparable performances for a similar technique also relying on UAV laser-based concentrations monitoring associated with a mass balance model (Morales et al., 2022).

This method has a wide range of potential applications, for the quantification of $CO_2$ or $CH_4$ sources of diverse anthropogenic or natural origins. It was already applied on the field and extended in 2022 to more than 100 oil and gas facilities, offshore and onshore, from tropical to high latitude environments, as well as biogas plants and

500   landfills, which will be the subject of upcoming publications.

Field applications of our method revealed several assets compared to similar quantification campaigns previously conducted from aircrafts or boats. Compared to aircraft-based monitoring, UAVs have the advantage to fly below 300 m high and close to the facilities (distance around 250 m from offshore platforms), allowing the monitoring of the entire plume and the identification of the main sources. The real time monitoring of the concentration on

505   the ground, associated with the high speed and reactivity of the UAV, provides the possibility for the pilots to adapt the trajectory and fly within the plume despite its meandering. The UAV high speed also allows monitoring of an entire plume within a few minutes, thus representative of a quasi-stationary state, preventing for example double measurements of the same plume when it is meandering, which could occur with measurements conducted from a low-speed vessel. The high frequency of observations (conducted at 24 Hz for these campaigns) allowed

510   us to develop an emissions quantification method which does not require a 2D interpolation of the measured concentration data, but only an interpolation along the vertical direction. This improves the precision compared to methods requiring 2D interpolation based on Kriging techniques.

Nevertheless, our quantifications would benefit from further improvements of the instruments, the monitoring protocol or the modelling.

515   Our mass balance method provides precise emissions quantifications at low computing costs, but requires concentration measurements throughout an entire plume cross-section. This is not always possible to perform on the field, due to restrictions of the UAV area of operations caused by obstacles or prohibited flight zones. An inverse atmospheric modelling method might provide emissions quantifications for partially monitored plume cross-sections.

520   A more precise recording of the horizontal and vertical UAV positioning has already been introduced with the use of RTK GPS positioning, facilitating data post-treatment. Future technical development of our method will include wind speed measurements directly on-board the UAV, replacing the LiDAR wind profile measurements for an easier and more cost-effective field deployment. This should also improve the wind speed measurements at elevations below the lowest level of wind LiDAR measurements (typically below 10 m.a.g.l.). A fully automatized

525   UAV operation is also being developed, with UAV track adapting to the plume position, aiming at regular quantifications of O&G facilities.

Future improvements will be made to our greenhouse gases sensor. CO concentrations measurements will also be included in future versions of our instrument, allowing the calculation of a complete combustion efficiency balance for various types of sources of the O&G sector, such as flares. Further weight reduction and adaptations of the

530 instrument will allow it to be embarked by a larger spectrum of air carriers, including VTOLs (Vertical Take-Off and Landing) UAVs, which have a longer autonomy and fly and higher speed. This will open new applications to monitor emissions of larger scale sources such as larger industrial facilities, natural sources or small cities.

**Author contribution**

The manuscript writing has been initiated by J.L.B., completed by N.G., L.D. and L.J. and corrected by all co-
535 authors. The AUSEA sensors and associated spectrometric inversion algorithms have been developed at the GSMA by L.J., J.C., T.D., J.B., N.C., N.D., G.A., F.P. In-lab validation of the AUSEA sensor has been performed by J.L.B. and D.C. Emissions quantification model development and computations were conducted by L.D., N.G. Field monitoring campaigns were conducted by A.M, O.V. and L.D.  The project has been initiated and coordinated by L.J. and L.D., O.D., C.J., M.F.B.

540 **Competing interests**

The authors declare that they have no conflict of interest.

**Acknowledgments**

The instrumental development and the quantification algorithm were funded via a collaboration between the GSMA laboratory of the Université de Reims Champagne-Ardenne (URCA) and the R&D LQA laboratory of
545 TotalEnergies, within the frame of the AUSEA project and the common laboratory LabCom LYNNA (hosted by CNRS, URCA and TotalEnergies).
Observations around offshore platforms were conducted from a supply boat chartered by TEPNL from Den Helder harbor. We thank the crew for their assistance and all the affiliated people that helped us to manage those experiments.
550 Participations to the TADI campaign were possible thanks to the facilities and assistance of the TotalEnergies TADI teams from the PERL (Pôle d'Etude et de Recherches de Lacq), who organised the controlled releases.

**References**

Allen, G., Hollingsworth, P., Kabbabe, K., Pitt, J. R., Mead, M. I., Illingworth, S., Roberts, G., Bourn, M., Shallcross, D. E., and Percival, C. J.: The development and trial of an unmanned aerial system for the measurement
555 of methane flux from landfill and greenhouse gas emission hotspots, Waste Manag., 87, 883–892, https://doi.org/10.1016/j.wasman.2017.12.024, 2019.

Alvarez, R. A., Zavala-Araiza, D., Lyon, D. R., Allen, D. T., Barkley, Z. R., Brandt, A. R., Davis, K. J., Herndon, S. C., Jacob, D. J., Karion, A., Kort, E. A., Lamb, B. K., Lauvaux, T., Maasakkers, J. D., Marchese, A. J., Omara, M., Pacala, S. W., Peischl, J., Robinson, A. L., Shepson, P. B., Sweeney, C., Townsend-Small, A., Wofsy, S. C.,
560 and Hamburg, S. P.: Assessment of methane emissions from the U.S. oil and gas supply chain, Science, 361, 186–188, https://doi.org/10.1126/science.aar7204, 2018.

Glasgow Climate Pact | UNFCCC: https://unfccc.int/documents/310475, last access: 2 December 2021.

NF EN 17628: https://www.boutique.afnor.org/fr-fr/norme/nf-en-17628/emissions-fugitives-et-diffuses-concernant-les-secteurs-industriels-methode/fa194272/325170, last access: 30 November 2022.

565 Oil and Gas Methane Partnership (OGMP) 2.0 Framework: https://www.ccacoalition.org/en/resources/oil-and-gas-methane-partnership-ogmp-20-framework, last access: 4 July 2022.

Ars, S., Broquet, G., Yver Kwok, C., Roustan, Y., Wu, L., Arzoumanian, E., and Bousquet, P.: Statistical atmospheric inversion of local gas emissions by coupling the tracer release technique and local-scale transport modelling: a test case with controlled methane emissions, Atmospheric Meas. Tech., 10, 5017–5037,
570 https://doi.org/10.5194/amt-10-5017-2017, 2017.

Berman, E. S. F., Fladeland, M., Liem, J., Kolyer, R., and Gupta, M.: Greenhouse gas analyzer for measurements of carbon dioxide, methane, and water vapor aboard an unmanned aerial vehicle, Sens. Actuators B Chem., 169, 128–135, https://doi.org/10.1016/j.snb.2012.04.036, 2012.

Brantley, H. L., Thoma, E. D., Squier, W. C., Guven, B. B., and Lyon, D.: Assessment of Methane Emissions from
575 Oil and Gas Production Pads using Mobile Measurements, Environ. Sci. Technol., 48, 14508–14515, https://doi.org/10.1021/es503070q, 2014.

Brereton, C. A., Joynes, I. M., Campbell, L. J., and Johnson, M. R.: Fugitive emission source characterization using a gradient-based optimization scheme and scalar transport adjoint, Atmos. Environ., 181, 106–116, https://doi.org/10.1016/j.atmosenv.2018.02.014, 2018.

580 Chen, H., Winderlich, J., Gerbig, C., Hoefer, A., Rella, C. W., Crosson, E. R., Van Pelt, A. D., Steinbach, J., Kolle, O., Beck, V., Daube, B. C., Gottlieb, E. W., Chow, V. Y., Santoni, G. W., and Wofsy, S. C.: High-accuracy continuous airborne measurements of greenhouse gases (CO2 and CH4) using the cavity ring-down spectroscopy (CRDS) technique, Atmos Meas Tech, 3, 375–386, https://doi.org/10.5194/amt-3-375-2010, 2010.

Conley, S., Franco, G., Faloona, I., Blake, D. R., Peischl, J., and Ryerson, T. B.: Methane emissions from the 2015
585 Aliso Canyon blowout in Los Angeles, CA, Science, 351, 1317–1320, https://doi.org/10.1126/science.aaf2348, 2016.

Conley, S., Faloona, I., Mehrotra, S., Suard, M., Lenschow, D. H., Sweeney, C., Herndon, S., Schwietzke, S., Pétron, G., Pifer, J., Kort, E. A., and Schnell, R.: Application of Gauss's theorem to quantify localized surface emissions from airborne measurements of wind and trace gases, Atmospheric Meas. Tech., 10, 3345–3358,
590 https://doi.org/10.5194/amt-10-3345-2017, 2017.

Crosson, E. R.: A cavity ring-down analyzer for measuring atmospheric levels of methane, carbon dioxide, and water vapor, Appl. Phys. B, 92, 403–408, https://doi.org/10.1007/s00340-008-3135-y, 2008.

Druart, G., Foucher, P.-Y., Doz, S., Watremez, X., Jourdan, S., Vanneau, E., and Pinot, H.: Test of SIMAGAZ: a LWIR cryogenic multispectral infrared camera for methane gas leak detection and quantification, in: Algorithms,
595 Technologies, and Applications for Multispectral and Hyperspectral Imaging XXVII, Algorithms, Technologies, and Applications for Multispectral and Hyperspectral Imaging XXVII, 53–59, https://doi.org/10.1117/12.2586933, 2021.

Dullo, F. T., Lindecrantz, S., Jágerská, J., Hansen, J. H., Engqvist, M., Solbø, S. A., and Hellesø, O. G.: Sensitive on-chip methane detection with a cryptophane-A cladded Mach-Zehnder interferometer, Opt. Express, 23, 31564–
600 31573, https://doi.org/10.1364/OE.23.031564, 2015.

Durry, G. and Megie, G.: Atmospheric $CH_4$ and $H_2O$ monitoring with near-infrared InGaAs laser diodes by the SDLA, a balloonborne spectrometer for tropospheric and stratospheric in situ measurements, Appl. Opt., 38, 7342–7354, https://doi.org/10.1364/AO.38.007342, 1999.

Etminan, M., Myhre, G., Highwood, E. J., and Shine, K. P.: Radiative forcing of carbon dioxide, methane, and
605 nitrous oxide: A significant revision of the methane radiative forcing, Geophys. Res. Lett., 43, 12,614-12,623, https://doi.org/10.1002/2016GL071930, 2016.

Feitz, A., Schroder, I., Phillips, F., Coates, T., Negandhi, K., Day, S., Luhar, A., Bhatia, S., Edwards, G., Hrabar, S., Hernandez, E., Wood, B., Naylor, T., Kennedy, M., Hamilton, M., Hatch, M., Malos, J., Kochanek, M., Reid, P., Wilson, J., Deutscher, N., Zegelin, S., Vincent, R., White, S., Ong, C., George, S., Maas, P., Towner, S., Wokker, N., and Griffith, D.: The Ginninderra CH4 and CO2 release experiment: An evaluation of gas detection and quantification techniques, Int. J. Greenh. Gas Control, 70, 202–224, https://doi.org/10.1016/j.ijggc.2017.11.018, 2018.

Fiehn, A., Kostinek, J., Eckl, M., Klausner, T., Galkowski, M., Chen, J., Gerbig, C., Röckmann, T., Maazallahi, H., Schmidt, M., Korben, P., Necki, J., Jagoda, P., Wildmann, N., Mallaun, C., Bun, R., Nickl, A.-L., Jöckel, P., Fix, A., and Roiger, A.: Estimating CH4, CO2 and CO emissions from coal mining and industrial activities in the Upper Silesian Coal Basin using an aircraft-based mass balance approach, ATMOSPHERIC Chem. Phys., 20, 12675–12695, https://doi.org/10.5194/acp-20-12675-2020, 2020.

Forster, P., Storelvmo, T., Armour, K., Collins, W., Dufresne, J.-L., Frame, D., Lunt, D., Mauritsen, T., Palmer, M., and Watanabe, M.: The Earth's energy budget, climate feedbacks, and climate sensitivity, in: Climate Change 2021: The Physical Science Basis. Contribution of Working Group I to the Sixth Assessment Report of the Intergovernmental Panel on Climate Change, Cambridge University Press, Oxford, UK, 923−1054, 2021.

France, J. L., Bateson, P., Dominutti, P., Allen, G., Andrews, S., Bauguitte, S., Coleman, M., Lachlan-Cope, T., Fisher, R. E., Huang, L., Jones, A. E., Lee, J., Lowry, D., Pitt, J., Purvis, R., Pyle, J., Shaw, J., Warwick, N., Weiss, A., Wilde, S., Witherstone, J., and Young, S.: Facility level measurement of offshore oil and gas installations from a medium-sized airborne platform: method development for quantification and source identification of methane emissions, Atmospheric Meas. Tech., 14, 71–88, https://doi.org/10.5194/amt-14-71-2021, 2021.

Golston, L. M., Tao, L., Brosy, C., Schäfer, K., Wolf, B., McSpiritt, J., Buchholz, B., Caulton, D. R., Pan, D., Zondlo, M. A., Yoel, D., Kunstmann, H., and McGregor, M.: Lightweight mid-infrared methane sensor for unmanned aerial systems, Appl. Phys. B, 123, 170, https://doi.org/10.1007/s00340-017-6735-6, 2017.

Golston, L. M., Aubut, N. F., Frish, M. B., Yang, S., Talbot, R. W., Gretencord, C., McSpiritt, J., and Zondlo, M. A.: Natural Gas Fugitive Leak Detection Using an Unmanned Aerial Vehicle: Localization and Quantification of Emission Rate, Atmosphere, 9, 333, https://doi.org/10.3390/atmos9090333, 2018.

Gorchov Negron, A. M., Kort, E. A., Conley, S. A., and Smith, M. L.: Airborne Assessment of Methane Emissions from Offshore Platforms in the U.S. Gulf of Mexico, Environ. Sci. Technol., 54, 5112–5120, https://doi.org/10.1021/acs.est.0c00179, 2020.

Hirst, B., Jonathan, P., González del Cueto, F., Randell, D., and Kosut, O.: Locating and quantifying gas emission sources using remotely obtained concentration data, Atmos. Environ., 74, 141–158, https://doi.org/10.1016/j.atmosenv.2013.03.044, 2013.

Hmiel, B., Petrenko, V. V., Dyonisius, M. N., Buizert, C., Smith, A. M., Place, P. F., Harth, C., Beaudette, R., Hua, Q., Yang, B., Vimont, I., Michel, S. E., Severinghaus, J. P., Etheridge, D., Bromley, T., Schmitt, J., Faïn, X., Weiss, R. F., and Dlugokencky, E.: Preindustrial 14 CH 4 indicates greater anthropogenic fossil CH 4 emissions, Nature, 578, 409–412, https://doi.org/10.1038/s41586-020-1991-8, 2020.

Huang, Z., Wang, Y., Yu, Q., Ma, W., Zhang, Y., and Chen, L.: Source area identification with observation from limited monitor sites for air pollution episodes in industrial parks, Atmos. Environ., 122, 1–9, https://doi.org/10.1016/j.atmosenv.2015.08.048, 2015.

ICOS RI: ICOS Atmosphere Station Specifications V2.0 (editor: O. Laurent), 2734778, https://doi.org/10.18160/GK28-2188, 2020.

Jackson, R. B., Down, A., Phillips, N. G., Ackley, R. C., Cook, C. W., Plata, D. L., and Zhao, K.: Natural Gas Pipeline Leaks Across Washington, DC, Environ. Sci. Technol., 48, 2051–2058, https://doi.org/10.1021/es404474x, 2014.

Joly, L., Maamary, R., Decarpenterie, T., Cousin, J., Dumelié, N., Chauvin, N., Legain, D., Tzanos, D., and Durry, G.: Atmospheric Measurements by Ultra-Light SpEctrometer (AMULSE) Dedicated to Vertical Profile in Situ

Measurements of Carbon Dioxide (CO2) Under Weather Balloons: Instrumental Development and Field Application, Sensors, 16, 1609, https://doi.org/10.3390/s16101609, 2016.

655 Joly, L., Coopmann, O., Guidard, V., Decarpenterie, T., Dumelié, N., Cousin, J., Burgalat, J., Chauvin, N., Albora, G., Maamary, R., Miftah El Khair, Z., Tzanos, D., Barrié, J., Moulin, É., Aressy, P., and Belleudy, A.: The development of the Atmospheric Measurements by Ultra-Light Spectrometer (AMULSE) greenhouse gas profiling system and application for satellite retrieval validation, Atmospheric Meas. Tech., 13, 3099–3118, https://doi.org/10.5194/amt-13-3099-2020, 2020.

660 Karion, A., Sweeney, C., Kort, E. A., Shepson, P. B., Brewer, A., Cambaliza, M., Conley, S. A., Davis, K., Deng, A., Hardesty, M., Herndon, S. C., Lauvaux, T., Lavoie, T., Lyon, D., Newberger, T., Pétron, G., Rella, C., Smith, M., Wolter, S., Yacovitch, T. I., and Tans, P.: Aircraft-Based Estimate of Total Methane Emissions from the Barnett Shale Region, Environ. Sci. Technol., 49, 8124–8131, https://doi.org/10.1021/acs.est.5b00217, 2015.

Khan, A., Schaefer, D., Tao, L., Miller, D. J., Sun, K., Zondlo, M. A., Harrison, W. A., Roscoe, B., and Lary, D. 665 J.: Low Power Greenhouse Gas Sensors for Unmanned Aerial Vehicles, Remote Sens., 4, 1355–1368, https://doi.org/10.3390/rs4051355, 2012.

Kumar, P., Broquet, G., Yver-Kwok, C., Laurent, O., Gichuki, S., Caldow, C., Cropley, F., Lauvaux, T., Ramonet, M., Berthe, G., Martin, F., Duclaux, O., Juery, C., Bouchet, C., and Ciais, P.: Mobile atmospheric measurements and local-scale inverse estimation of the location and rates of brief $CH_4$ and $CO_2$ releases from point sources, 670 Atmospheric Meas. Tech., 14, 5987–6003, https://doi.org/10.5194/amt-14-5987-2021, 2021.

Kumar, P., Broquet, G., Caldow, C., Laurent, O., Gichuki, S., Cropley, F., Yver-Kwok, C., Fontanier, B., Lauvaux, T., Ramonet, M., Shah, A., Berthe, G., Martin, F., Duclaux, O., Juery, C., Bouchet, C., Pitt, J., and Ciais, P.: Near-field atmospheric inversions for the localization and quantification of controlled methane releases using stationary and mobile measurements, Q. J. R. Meteorol. Soc., 148, 1886–1912, https://doi.org/10.1002/qj.4283, 2022.

675 Lee, J. D., Mobbs, S. D., Wellpott, A., Allen, G., Burton, R. R., Camilli, R., Coe, H., Fisher, R. E., France, J. L., Gallagher, M. W., Hopkins, J. R., Lanoiselle, M., Lewis, A. C., Lowry, D., Nisbet, E. G., Purvis, R. M., O'Shea, S., Pyle, J. A., and Ryerson, T. B.: Flow rate and source reservoir identification from airborne chemical sampling of the uncontrolled Elgin platform gas release, Atmospheric Meas. Tech., 1725–1739, 2018.

Liu, S., Yang, X., and Zhou, X.: Development of a low-cost UAV-based system for CH4 monitoring over oil 680 fields, Environ. Technol., 1–10, https://doi.org/10.1080/09593330.2020.1724199, 2020.

Malaver, A., Motta, N., Corke, P., and Gonzalez, F.: Development and Integration of a Solar Powered Unmanned Aerial Vehicle and a Wireless Sensor Network to Monitor Greenhouse Gases, Sensors, 15, 4072–4096, https://doi.org/10.3390/s150204072, 2015.

Masson-Delmotte, V., Zhai, P., Pörtner, H. O., Roberts, D., Skea, J., Shukla, P. R., Pirani, A., Moufouma-Okia, 685 W., Péan, C., and Pidcock, R.: IPCC, 2018: Summary for Policymakers. In: Global warming of 1.5 C. An IPCC Special Report on the impacts of global warming of 1.5 C above pre-industrial levels and related global greenhouse gas emission pathways, in the context of strengthening the global, World Meteorol. Organ. Geneva Tech Rep, 2018.

Mays, K. L., Shepson, P. B., Stirm, B. H., Karion, A., Sweeney, C., and Gurney, K. R.: Aircraft-Based 690 Measurements of the Carbon Footprint of Indianapolis, Environ. Sci. Technol., 43, 7816–7823, https://doi.org/10.1021/es901326b, 2009.

Mønster, J., Kjeldsen, P., and Scheutz, C.: Methodologies for measuring fugitive methane emissions from landfills – A review, Waste Manag., 87, 835–859, https://doi.org/10.1016/j.wasman.2018.12.047, 2019.

Morales, R., Ravelid, J., Vinkovic, K., Korbeń, P., Tuzson, B., Emmenegger, L., Chen, H., Schmidt, M., Humbel, 695 S., and Brunner, D.: Controlled-release experiment to investigate uncertainties in UAV-based emission quantification for methane point sources, Atmospheric Meas. Tech., 15, 2177–2198, https://doi.org/10.5194/amt-15-2177-2022, 2022.

Nara, H., Tanimoto, H., Tohjima, Y., Mukai, H., Nojiri, Y., and Machida, T.: Emissions of methane from offshore oil and gas platforms in Southeast Asia, Sci. Rep., 4, 6503, https://doi.org/10.1038/srep06503, 2014.

700 Nathan, B. J., Golston, L. M., O'Brien, A. S., Ross, K., Harrison, W. A., Tao, L., Lary, D. J., Johnson, D. R., Covington, A. N., Clark, N. N., and Zondlo, M. A.: Near-Field Characterization of Methane Emission Variability from a Compressor Station Using a Model Aircraft, Environ. Sci. Technol., 49, 7896–7903, https://doi.org/10.1021/acs.est.5b00705, 2015.

Neumann, P. P., Bennetts, V. H., Lilienthal, A. J., Bartholmai, M., and Schiller, J. H.: Gas source localization with
705 a micro-drone using bio-inspired and particle filter-based algorithms, Adv. Robot., 27, 725–738, https://doi.org/10.1080/01691864.2013.779052, 2013.

Ng, R. T. L., Hassim, M. H., and Hurme, M.: A hybrid approach for estimating fugitive emission rates in process development and design under incomplete knowledge, Process Saf. Environ. Prot., 109, 365–373, https://doi.org/10.1016/j.psep.2017.04.003, 2017.

710 O'Keefe, A.: Integrated cavity output analysis of ultra-weak absorption, Chem. Phys. Lett., 293, 331–336, https://doi.org/10.1016/S0009-2614(98)00785-4, 1998.

O'Keefe, A., Scherer, J. J., and Paul, J. B.: cw Integrated cavity output spectroscopy, Chem. Phys. Lett., 307, 343–349, https://doi.org/10.1016/S0009-2614(99)00547-3, 1999.

Ravikumar, A. P., Sreedhara, S., Wang, J., Englander, J., Roda-Stuart, D., Bell, C., Zimmerle, D., Lyon, D.,
715 Mogstad, I., Ratner, B., and Brandt, A. R.: Single-blind inter-comparison of methane detection technologies – results from the Stanford/EDF Mobile Monitoring Challenge, Elem. Sci. Anthr., 7, https://doi.org/10.1525/elementa.373, 2019.

Rella, C.: Accurate greenhouse gas measurements in humid gas streams using the Picarro G1301 carbon dioxide/methane/water vapor gas analyzer, White Pap. Picarro Inc Sunnyvale CA USA, 2010.

720 Riddick, S. N., Mauzerall, D. L., Celia, M., Harris, N. R. P., Allen, G., Pitt, J., Staunton-Sykes, J., Forster, G. L., Kang, M., Lowry, D., Nisbet, E. G., and Manning, A. J.: Methane emissions from oil and gas platforms in the North Sea, Atmospheric Chem. Phys., 19, 9787–9796, https://doi.org/10.5194/acp-19-9787-2019, 2019.

Rivera Martinez, R., Santaren, D., Laurent, O., Cropley, F., Mallet, C., Ramonet, M., Caldow, C., Rivier, L., Broquet, G., Bouchet, C., Juery, C., and Ciais, P.: The Potential of Low-Cost Tin-Oxide Sensors Combined with
725 Machine Learning for Estimating Atmospheric CH4 Variations around Background Concentration, Atmosphere, 12, 107, https://doi.org/10.3390/atmos12010107, 2021.

Romanini, D., Chenevier, M., Kassi, S., Schmidt, M., Valant, C., Ramonet, M., Lopez, J., and Jost, H.-J.: Optical–feedback cavity–enhanced absorption: a compact spectrometer for real–time measurement of atmospheric methane, Appl. Phys. B, 83, 659–667, https://doi.org/10.1007/s00340-006-2177-2, 2006.

730 Saunois, M., Stavert, A. R., Poulter, B., Bousquet, P., Canadell, J. G., Jackson, R. B., Raymond, P. A., Dlugokencky, E. J., Houweling, S., Patra, P. K., Ciais, P., Arora, V. K., Bastviken, D., Bergamaschi, P., Blake, D. R., Brailsford, G., Bruhwiler, L., Carlson, K. M., Carrol, M., Castaldi, S., Chandra, N., Crevoisier, C., Crill, P. M., Covey, K., Curry, C. L., Etiope, G., Frankenberg, C., Gedney, N., Hegglin, M. I., Höglund-Isaksson, L., Hugelius, G., Ishizawa, M., Ito, A., Janssens-Maenhout, G., Jensen, K. M., Joos, F., Kleinen, T., Krummel, P. B.,
735 Langenfelds, R. L., Laruelle, G. G., Liu, L., Machida, T., Maksyutov, S., McDonald, K. C., McNorton, J., Miller, P. A., Melton, J. R., Morino, I., Müller, J., Murguia-Flores, F., Naik, V., Niwa, Y., Noce, S., O'Doherty, S., Parker, R. J., Peng, C., Peng, S., Peters, G. P., Prigent, C., Prinn, R., Ramonet, M., Regnier, P., Riley, W. J., Rosentreter, J. A., Segers, A., Simpson, I. J., Shi, H., Smith, S. J., Steele, L. P., Thornton, B. F., Tian, H., Tohjima, Y., Tubiello, F. N., Tsuruta, A., Viovy, N., Voulgarakis, A., Weber, T. S., van Weele, M., van der Werf, G. R., Weiss, R. F.,
740 Worthy, D., Wunch, D., Yin, Y., Yoshida, Y., Zhang, W., Zhang, Z., Zhao, Y., Zheng, B., Zhu, Q., Zhu, Q., and Zhuang, Q.: The Global Methane Budget 2000–2017, Earth Syst. Sci. Data, 12, 1561–1623, https://doi.org/10.5194/essd-12-1561-2020, 2020.

Shah, A., Pitt, J. R., Ricketts, H., Leen, J. B., Williams, P. I., Kabbabe, K., Gallagher, M. W., and Allen, G.: Testing the near-field Gaussian plume inversion flux quantification technique using unmanned aerial vehicle sampling, Atmospheric Meas. Tech., 13, 1467–1484, https://doi.org/10.5194/amt-13-1467-2020, 2020.

Shindell, D., Kuylenstierna, J. C. I., Vignati, E., Dingenen, R. van, Amann, M., Klimont, Z., Anenberg, S. C., Muller, N., Janssens-Maenhout, G., Raes, F., Schwartz, J., Faluvegi, G., Pozzoli, L., Kupiainen, K., Höglund-Isaksson, L., Emberson, L., Streets, D., Ramanathan, V., Hicks, K., Oanh, N. T. K., Milly, G., Williams, M., Demkine, V., and Fowler, D.: Simultaneously Mitigating Near-Term Climate Change and Improving Human Health and Food Security, Science, 335, 183–189, https://doi.org/10.1126/science.1210026, 2012.

Terry, C., Argyle, M., Meyer, S., Sander, L., and Hirst, B.: Mapping methane sources and their emission rates using an aircraft, Lead. Edge, 36, 33–35, https://doi.org/10.1190/tle36010033.1, 2017.

Tuzson, B., Graf, M., Ravelid, J., Scheidegger, P., Kupferschmid, A., Looser, H., Morales, R. P., and Emmenegger, L.: A compact QCL spectrometer for mobile, high-precision methane sensing aboard drones, Atmospheric Meas. Tech., 13, 4715–4726, https://doi.org/10.5194/amt-13-4715-2020, 2020.

Worden, J. R., Bloom, A. A., Pandey, S., Jiang, Z., Worden, H. M., Walker, T. W., Houweling, S., and Röckmann, T.: Reduced biomass burning emissions reconcile conflicting estimates of the post-2006 atmospheric methane budget, Nat. Commun., 8, 2227, https://doi.org/10.1038/s41467-017-02246-0, 2017.

Xia, J., Zhu, F., Zhang, S., Kolomenskii, A., and Schuessler, H.: A ppb level sensitive sensor for atmospheric methane detection, Infrared Phys. Technol., 86, 194–201, https://doi.org/10.1016/j.infrared.2017.09.018, 2017.

Yacovitch, T. I., Daube, C., and Herndon, S. C.: Methane Emissions from Offshore Oil and Gas Platforms in the Gulf of Mexico, Environ. Sci. Technol., 54, 3530–3538, https://doi.org/10.1021/acs.est.9b07148, 2020.

Yver Kwok, C., Laurent, O., Guemri, A., Philippon, C., Wastine, B., Rella, C. W., Vuillemin, C., Truong, F., Delmotte, M., Kazan, V., Darding, M., Lebègue, B., Kaiser, C., Xueref-Rémy, I., and Ramonet, M.: Comprehensive laboratory and field testing of cavity ring-down spectroscopy analyzers measuring $H_2O$, $CO_2$, $CH_4$ and CO, Atmospheric Meas. Tech., 8, 3867–3892, https://doi.org/10.5194/amt-8-3867-2015, 2015.

745

750

755

760

765

**Figure 1. Picture of the AUSEA 112 analyzer mounted on a DJI M300.**
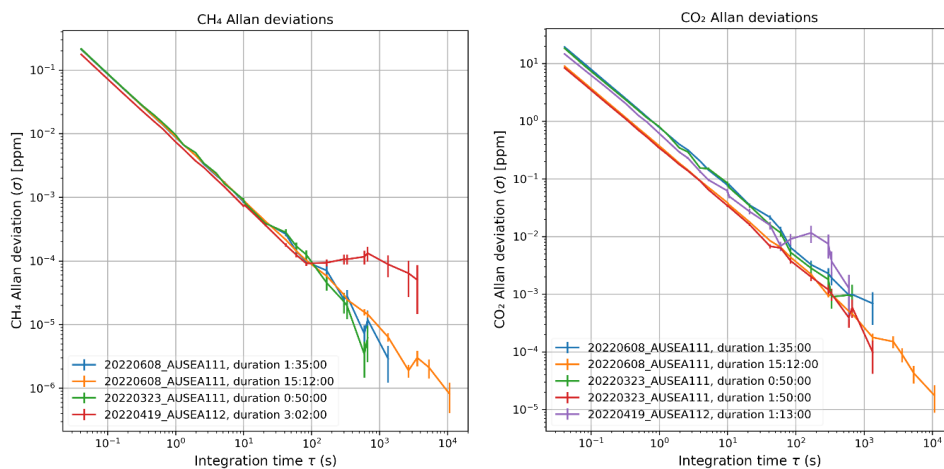
770

**Figure 2 Allan deviations calculated for multiple stability experiments with analysers AUSEA_111 and AUSEA_112.**
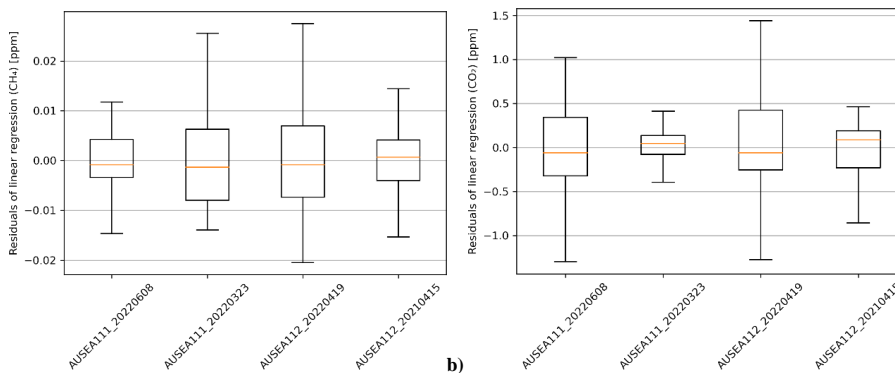
Figure 3. Boxplots of the residuals of the linear regressions for each linearity experiment of the AUSEA sensor against
a reference Picarro CRDS analyser in a temperature-controlled environment at a 5 s temporal resolution. Boxplots
775    depict the first and last quartile (lower and upper borders of the boxes), median (orange line) and minima and maxima
(lower and upper ticks, defined as the first and last quartile plus or minus 1.5 times the interquartile range), without
outliers.
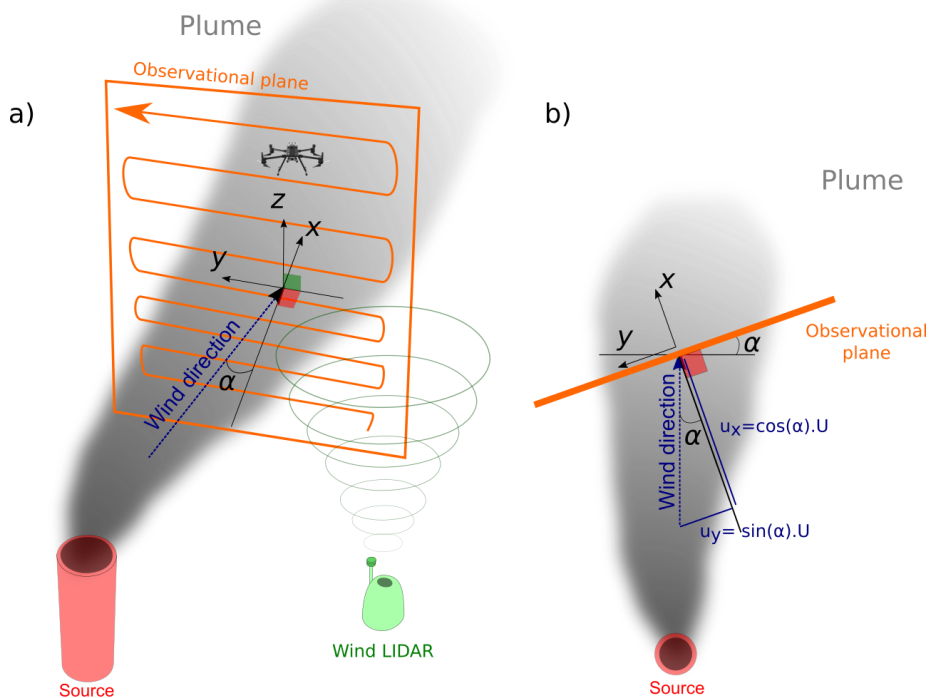
**Figure 4. Schematic representation of the observation protocol: general 3D view (a) and top view (b). The source (in red) emits a plume (grey shade). The UAV monitors the concentrations along a flight path (orange arrow), constituted of multiple horizontal transects, within a vertical observational plane, represented by the orange quadrangle in (a) and the orange line in (b). The angle between the orthogonal to the observational plane and the wind direction is noted $\alpha$. A wind LiDAR (green) measures the wind direction and speed at several elevations.**

785    **Figure 5. Aerial view of the TADI platform with location of the emission sources (yellow crosses) and the Explosive Atmosphere area (ATEX zone, depicted as an orange square). Maps Data: Google, ©2022 Maxar Technologies.**
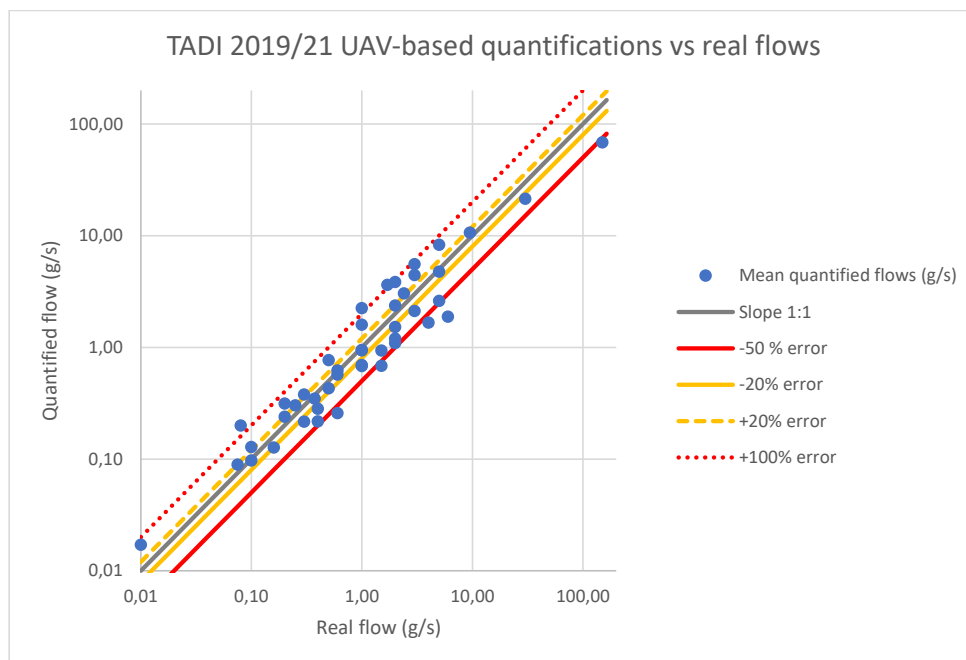
**Figure 6. Comparison of emissions quantifications as a function of the real CH₄ emissions fluxes (in g/s), as blue dots. A log-log scale is used. The plain grey line indicates the 1/1 slope or 0% error. Plain and dashed yellow lines respectively**

790 **indicate the -20 % and +20 % relative errors limits. Plain and dotted red lines respectively indicate the -50 % and +100 % error limits.**

**Figure 7 : Picture of operations nearby offshore platforms in the North Sea on 2019-04-19, showing (a) the UAV equipped with the AUSEA sensor and (b) the deck of the supply vessel serving as take-off and landing site for the UAV,**

795 **with the wind LiDAR (black circle).**
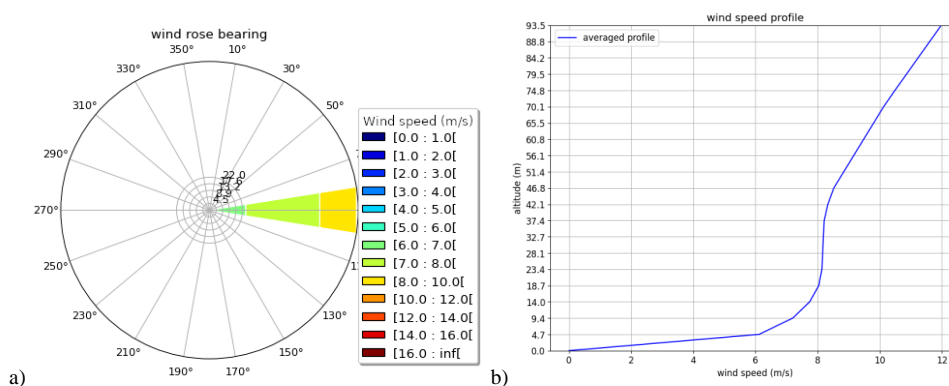
**Figure 8. Typical weather conditions for flight 2_P2 of the offshore platform monitoring campaign: a) Distributions of wind directions (percentage, with 20° resolution) for different wind speeds classes (color scale, in m/s) during flight measured by the LiDAR at the lowest level. b) Averaged wind speed (m/s) vertical profile (in m.a.s.l) over the flight duration, measured by wind LiDAR at each of its monitoring level.**

| Instrument | Date | Duration | Species (unit) | $\sigma_{0.5\,s}$ | $\sigma_{1\,s}$ | $\sigma_{10\,s}$ | $\sigma_{60s}$ |
|---|---|---|---|---|---|---|---|
| AUSEA111 | 2022-06-08 | 1 h 35 min | $CH_4$ | 18 | 9 | 0.8 | 0.1 |
| AUSEA111 | 2022-06-08 | 15 h 12 min | (ppb) | 18 | 9 | 0.9 | 0.1 |
| AUSEA111 | 2022-03-23 | 50 min | | 19 | 10 | 0.9 | 0.2 |
| AUSEA112 | 2022-04-19 | 3h 2 min | | 15 | 8 | 0.7 | 0.1 |
| AUSEA111 | 2022-06-08 | 1 h 35 min | $CO_2$ | 1.6 | 0.8 | 0.1 | 0.01 |
| AUSEA111 | 2022-06-08 | 15 h 12 min | (ppm) | 0.8 | 0.4 | 0.04 | 0.01 |
| AUSEA111 | 2022-03-23 | 50 min | | 1.5 | 0.8 | 0.1 | 0.01 |
| AUSEA111 | 2022-03-23 | 1 h 50 min | | 0.7 | 0.3 | 0.03 | 0.01 |
| AUSEA112 | 2022-04-19 | 1h 13 min | | 1.3 | 0.6 | 0.06 | 0.01 |

**Table 1 : Precisions of the AUSEA111 and AUSEA112 analyzers at given frequencies (0.5 s, 1 s, 10 s, 60 s) derived from Allan deviations of stability experiments performed at different dates, expressed in ppb for $CH_4$ and ppm for $CO_2$.**

| Instrument | Date | Species | Minimum (ppm) | Maximum (ppm) | Slope | Intercept (ppm) | $R^2$ | N |
|---|---|---|---|---|---|---|---|---|
| AUSEA112 | 2021-04-15 | $CH_4$ | 2.1 | 20.0 | 1.009 | +0.03 | 1.0 | 30751 |
| | 2022-04-19 | | 2.2 | 20.0 | 1.032 | +0.163 | 1.0 | 17169 |
| AUSEA111 | 2022-03-23 | | 3.2 | 20.0 | 1.008 | -0.018 | 1.0 | 16267 |
| | 2022-06-08 | | 2.2 | 20.0 | 0.991 | +0.024 | 1.0 | 5943 |
| AUSEA112 | 2021-04-15 | $CO_2$ | 429.0 | 509.9 | 1.007 | +6.538 | 1.0 | 30751 |
| | 2022-04-19 | | 454.9 | 646.3 | 1.009 | +6.2 | 1.0 | 17169 |
| AUSEA111 | 2022-03-23 | | 465.3 | 657.8 | 1.011 | +10.702 | 1.0 | 16267 |
| | 2022-06-08 | | 532.3 | 861.4 | 0.995 | +17.7656 | 1.0 | 5943 |

**Table 2 : Results of the linearity experiments for instruments AUSEA111 and AUSEA112 performed at different dates, for the $CH_4$ and $CO_2$ measurements: range of concentrations covered by the experiments (minimum and maximum**

**values), slope and intercept of the linear regressions of the distributions (only values below 20.0 ppm for $CH_4$) and associated $R^2$ values and number of data points at a 5 seconds frequency resolution used for the linear regression.**

| Quantifications relative errors (%) | | | | | Number of experiments |
|---|---|---|---|---|---|
| **Median** | **Average** | **σ** | **Minimum** | **Maximum** | |
| **With 1 quantification flight** | | | | | |
| -28% | -8% | 53% | -58% | 125% | 19 |
| **With 2 quantifications flights** | | | | | |
| 12% | 17% | 57% | -69% | 149% | 19 |
| **With 3 quantifications flights** | | | | | |
| 27% | 23% | 49% | -32% | 70% | 4 |
| **With 4 quantifications flights** | | | | | |
| 19% | 21% | 4% | 19% | 26% | 3 |
| **All quantifications** | | | | | |
| **-5%** | **7%** | **53%** | **-69%** | **149%** | **45** |

**Table 3. Statistics of the relative errors of quantifications during the TADI campaigns, for the release experiments quantified by 1, 2, 3 or 4 independent flights and for the total of all quantifications.**

| | | Real emitted fluxes categories (g/s) | | | | | |
|---|---|---|---|---|---|---|---|
| | | **[0,01-0,3[** | **[0,3-1[** | **[1-2[** | **[2-5[** | **[5-151[** | **[0,01-151]** |
| | **Average relative error (%)** | 38% | -10% | 15% | 7% | -18% | |
| **Relative error categories** | **[-20% : +20%[** | 3 | 3 | 2 | 1 | 2 | 11 |
| | **[-50% : +100%[** | 8 | 8 | 6 | 9 | 5 | 36 |
| | **[-69% : +150%[** | 9 | 10 | 9 | 10 | 7 | 45 |

810 **Table 4. Statistics of the quantifications results for different categories of real emitted fluxes: between 0.01 and 0.3 g/s, between 0.3 and 1 g/s, between 1 and 2 g/s, between 2 and 5 g/s, between 5 and 151 g/s and for the whole range between 0.01 and 151 g/s. The average relative error is given in % for each category, as well as the number of controlled release experiments for which the quantifications reached relative error categories between -20 and +20 %, between -50 and +100 % and between -69 % and +150 %. Underlined numbers correspond to the total number of controlled release**
815 **experiment within each real emitted flux category.**

| | Relative errors to site calculations (%) | | | |
| --- | --- | --- | --- | --- |
| Species | $CO_2$ | | $CH_4$ | |
| Platform (number of flights) | P1 (7 flights) | P2 (4 flights) | P1 (7 flights) | P2 (6 flights) |
| Minimum | -39% | -28% | 8% | -60% |
| 1st Quartile | -36% | -26% | 28% | -33% |
| Median | -23% | -19% | 32% | -21% |
| 3rd Quartile | -12% | -9% | 51% | -17% |
| Maximum | 14% | 2% | 128% | 229% |
| **Mean** | **-21%** | **-16%** | **46%** | **12%** |

**Table 5. Statistics of the distribution of quantified emissions for all 7 flights associated to each platform P1 and P2, for $CO_2$ and $CH_4$, expressed as relative differences (in %) to the reference daily average emission rates obtained by mass**
820 **balance and combustion efficiency calculations.**